Mode and Transport Studies of Laser-Cooled Ion Plasmas in a Penning Trap*

T. B. Mitchell, J. J. Bollinger, X.-P. Huang and W. M. Itano

Time and Frequency Division, National Institute of Standards and Technology, Boulder, CO 80303

Abstract. We describe a technique and present results for imaging the modes of a laser-cooled plasma of $^9\text{Be}^+$ ions in a Penning trap. The modes are excited by sinusoidally time-varying potentials applied to the trap electrodes, or by static field errors. They are imaged by changes in the ion resonance fluorescence produced by Doppler shifts from the coherent ion velocities of the mode. For the geometry and conditions of this experiment, the mode frequencies and eigenfunctions have been calculated analytically. A comparison between theory and experiment for some of the azimuthally symmetric modes shows good agreement. Enhanced radial transport is observed where modes are resonant with static external perturbations, such as those caused by misaligning the trap with respect to the magnetic field. Similarly, the plasma angular momentum can be changed through the deliberate excitation of azimuthally asymmetric modes. The resultant torque can be much greater than that from the "rotating wall" perturbation, which is not mode-resonant.

INTRODUCTION

Non-neutral plasmas consisting exclusively of particles of a single sign of charge have been used to study many basic processes in plasma physics [1], partly because non-neutral (as opposed to neutral or quasi-neutral) plasmas can be confined by static electric and magnetic fields and also be in a state of global thermal equilibrium [2,3]. A particularly simple confinement geometry for non-neutral plasmas is the quadratic Penning trap, which uses a strong uniform magnetic field $\mathbf{B_0} = B_0\hat{\mathbf{z}}$ superimposed on a quadratic electrostatic potential

$$\phi_T(r, z) = \frac{m\omega_z^2}{2q}\left(z^2 - \frac{r^2}{2}\right).\tag{1}$$

Here m and q are the mass and charge of a trapped ion, and ω_z is the axial frequency of a single ion in the trap. The global thermal equilibrium state for a single charged species in a quadratic Penning trap has been well studied [3,4]. For sufficiently low temperatures, the plasma takes on the simple shape of a uniform density spheroid. An interesting result is that all of the electrostatic modes of a magnetized, uniform density spheroidal plasma can be calculated analytically [5,6]. This is the only finite length geometry for which exact plasma mode frequencies and eigenfunctions have been calculated for a realistic thermal equilibrium state.

In this manuscript we describe a technique for measuring these frequencies and eigenfunctions, and compare theory predictions and experimental results for some of the magnetized plasma modes. We also discuss several potential applications for the modes in Penning trap experiments. In general, the mode frequencies depend on the density and shape of the plasma spheroid. Therefore measurement of a mode frequency provides a non-destructive method for obtaining basic diagnostic information about the plasma. This is especially important in anti-matter plasmas [7,8], where conventional techniques for obtaining information about these plasmas involve ejecting the plasma from the trap. Measurement of the damping of the modes can provide information on the plasma's viscosity [9,10]. Other applications arise from the fact that the modes can strongly influence the dynamical behavior of trapped plasmas. For example, certain azimuthally asymmetric modes can have zero frequency in the laboratory frame and be excited by a static field error of the trap. These zero-frequency modes can strongly limit the achievable density in a Penning trap [11]. Similarly, the plasma angular momentum can

---

be changed through the deliberate excitation of azimuthally asymmetric modes [12,13], and the applied torque can be much greater than that from the "rotating wall" perturbation [14,15], which is not mode-resonant.

Previous experimental mode studies on spheroidal plasmas have been limited to frequency measurements on a small class of modes. With laser-cooled Be^+ ion plasmas, some quadrupole mode frequencies have been measured and agree well with theory [6,11]. Mode frequencies have also been measured on spheroidal cryogenic electron plasmas [16], 0.025–0.5 eV electron and positron plasmas [17], and room temperature Ar^+ ion plasmas [18]. In these cases qualitative agreement with theory was observed and the modes provided some basic diagnostic information. However, deviations from the model of a constant density spheroid in a quadratic trap limited the comparison with the ideal linear theory. Here, in addition to measuring mode frequencies, we also measure the mode eigenfunctions. The eigenfunctions permit direct identification of the modes. In addition, they contain much more information than the frequencies and therefore may be useful for observing nonlinear effects such as mode couplings. Mode eigenfunctions have been measured for low frequency, z-independent (diocotron) modes on cylindrical electron columns [19]. In that work, the mode measurements were important in identifying two coexisting modes.

EXPERIMENTAL APPARATUS

Figure 1 shows a schematic of the apparatus [20,21] used for the mode measurements. The trap consists of a 127 mm long stack of cylindrical electrodes at room temperature with an inner diameter of 40.6 mm, enclosed in a 10^{-8} Pa vacuum chamber. A uniform magnetic field $B_0 = 4.465$ T is aligned parallel to the trap axis within $0.01°$, and results in a $^9Be^+$ cyclotron frequency $\Omega = qB_0/m = 2\pi \times 7.608$ MHz. The magnetic field is aligned by minimizing the excitation of zero-frequency modes produced by a tilt of the magnetic field with respect to the trap electrode symmetry axis [6,11]. Positive ions are confined in this trap by biasing the central ring electrode to a negative voltage $-V_0$ with respect to the endcaps. Because the dimensions of the Be^+ plasmas ($\lesssim 2$ mm) are small compared to the diameter of the trap electrodes, the quadratic potential of Eq. (1) is a good approximation for the trap potential. For most of the work reported here, V_0 was set at 2.00 kV which results in $\omega_z = 2\pi \times 1.13$ MHz and a single-particle magnetron frequency $\omega_m = [\Omega - (\Omega^2 - 2\omega_z^2)^{\frac{1}{2}}]/2 = 2\pi \times 84.9$ kHz.

We create a Be^+ plasma by ionizing neutral Be atoms in a separate trap (not shown) and then transferring
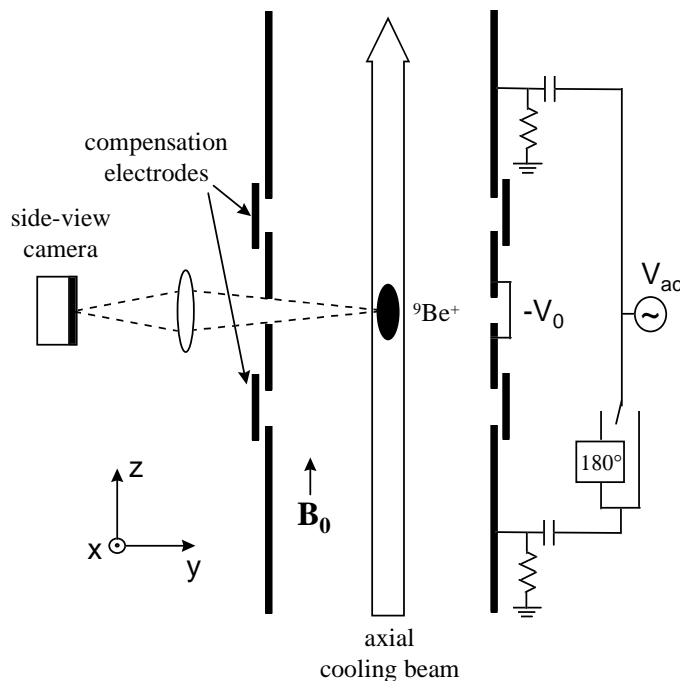
FIGURE 1. Schematic of the experimental apparatus. Azimuthally symmetric $m = 0$ modes were excited by applying in-phase or $180°$ out-of-phase sinusoidal potentials to the trap endcaps.

the ions to the main trap. For the work discussed here, the number of ions was typically 6×10^4. While the total charge in the trap is conserved after loading, the relative abundance of contaminant, heavier-mass ions increases, presumably due to reactions between Be^+ ions and background neutral molecules. Because we analyze our experimental results using an existing theory [5] for the electrostatic modes of a single-species plasma, we took data for mode studies only with relatively clean clouds (<3% impurity ions). The plasmas were cleaned approximately every 30 minutes by transferring the ions to the load trap where, with a shallow 3 V deep well, contaminant ions were driven out of the trap by exciting their axial frequencies. Cleaning therefore results in a decrease in the number of trapped ions. Over a 12–14 hour period, the number of ions is reduced by a factor of 2. Because the mode frequencies and eigenfunctions in a quadratic trap are independent of the number of ions, the mode measurements described here are not affected.

The trapped Be^+ ions are Doppler cooled by two laser beams at wavelength $\lambda \approx 313.11$ nm. The main cooling beam is directed parallel to $\mathbf{B_0}$ as shown in Fig. 1, and a second cooling beam propagating perpendicular to $\mathbf{B_0}$ (not shown and turned off during measurements) is also used to compress the plasma by applying a radiation pressure torque [3,11]. For mode eigenfunction measurements the axial cooling-laser frequency is fixed about one natural linewidth (~ 20 MHz) below the transition frequency. Ions which, due to excitation of a mode, have an axial velocity $v_z < 0$ therefore fluoresce more strongly than ions with $v_z > 0$. The ion temperature was not measured; however, based on previous work [3], we expect $T \lesssim 20$ mK.

An $f/5$ imaging system detects the Be^+ resonance fluorescence scattered perpendicularly from the axial cooling beam (waist ≈ 0.5 mm, power ≈ 50 μW) to produce a side-view image of the Be^+ ions. The side-view image is obtained with a photon-counting camera system which records the spatial and temporal coordinates of the detected photons. This data is processed to obtain the mode eigenfunctions by constructing side-view images as a function of the phase of the external drive used to excite the modes.

ELECTROSTATIC MODES OF A SPHEROIDAL PLASMA

A constant-density, spheroidal plasma model is a good approximation for our work. In thermal equilibrium, a Penning trap plasma rotates as a rigid body at frequency ω_r, where $\omega_m < \omega_r < \Omega - \omega_m$, about the trap's $\hat{\mathbf{z}}$ axis [2,4]. In this work the rotation frequency was precisely set by a rotating dipole electric field [14,15]. As the ions rotate through the magnetic field they experience a Lorentz force which provides the radial confining force of the trap. This ω_r-dependent confinement results in an ω_r-dependent ion density and plasma shape. At the low temperatures of this work, the plasma density is uniform over distances large compared to the interparticle spacing (~ 10 μm) and is given by $n_0 = \epsilon_0 m \omega_p^2/q^2$ where $\omega_p = [2\omega_r(\Omega - \omega_r)]^{\frac{1}{2}}$ is the plasma frequency. With the confining potential of Eq. (1), the plasma is spheroidal with boundary $z^2/z_0^2 + x^2/r_0^2 + y^2/r_0^2 = 1$. The spheroid aspect ratio $\alpha \equiv z_0/r_0$ is determined by ω_r [3,4]. We have neglected the effect of image charges, because the plasma dimensions are small compared to the trap dimensions.

The modes of these spheroidal plasmas can be classified by integers (l, m), where $l \geq 1$ and $0 \leq m \leq l$ [5,6]. For an (l, m) mode with frequency ω_{lm} [22] the perturbed potential of the mode inside the plasma is given by a symmetric product of Legendre functions,

$$\Psi^{lm} \propto P_l^m(\bar{\xi}_1/\bar{d})P_l^m(\bar{\xi}_2)e^{i(m\phi - \omega_{lm}t)}. \tag{2}$$

Here $\bar{\xi}_1$ and $\bar{\xi}_2$, discussed in Ref. [5], are scaled spheroidal coordinates where the scaling factor depends on the frequencies ω_r, Ω, and ω_{lm}, and $\bar{d}$ is a shape-dependent parameter which also depends on these frequencies. In general, for a given (l, m) there are many different modes. In this paper we report measurements of the mode frequencies and eigenfunctions of several magnetized plasma modes, which are defined as those modes with frequencies $|\omega_{lm}| < |\Omega - 2\omega_r|$ [5,6]. For $\omega_r \ll \Omega/2$, these modes principally consist of oscillations parallel to the magnetic field at a frequency on the order of ω_z. In the experiment we detect the axial velocity of a mode. In the linear theory, this is proportional to $\partial \Psi^{lm}/\partial z$.

We excite azimuthally symmetric ($m = 0$) plasma modes by applying sinusoidally time-varying potentials to the trap electrodes. Even-l $(l, 0)$ modes are excited by applying in-phase potentials to the endcaps (even drive), while odd-l $(l, 0)$ modes are excited by applying 180° out-of-phase potentials to the endcaps (odd drive). Azimuthally asymmetric ($m \neq 0$) modes can be excited by applying potentials to the compensation electrodes, which have 6-fold azimuthal symmetry. In Refs. [6,11] quadrupole ($l = 2$) mode frequencies were measured by observing the change in the total ion fluorescence from the plasma, averaged over the phase of the drive, which occurred when the drive frequency equaled the mode frequency. However, in order to observe such a change, the mode excitation must be large enough so that either the fluorescence from an ion nonlinearly depends on

its velocity or there is some heating of the plasma by the mode. The large amplitude drive required by this technique decreases the precision of the mode measurements.

The technique described here entails reducing the drive amplitude until the change in the phase-averaged ion fluorescence is negligible, and detecting the mode's coherent ion velocities by recording side-view images as a function of the phase and frequency of the external drive [23]. These Doppler images provide direct measurements of the mode's axial-velocity eigenfunction [24]. In addition, an accurate measurement of the mode's frequency (both real and imaginary parts) can be obtained from measurements of the mode amplitude as a function of drive frequency. High order modes have been excited and detected with this technique, such as the $(11,0)$ and $(12,1)$ modes. Imaging is not required for the $(1,0)$ and $(1,1)$ modes because there is no spatial variation in their eigenfunction. The driven mode amplitude and phase of these center-of-mass modes can therefore be obtained by coherently detecting the spatially integrated fluorescence as a function of the phase of the external drive [25].

EXPERIMENTAL RESULTS

Mode Frequency And Eigenfunction Measurements

In Fig. 2 we plot measured mode frequencies, along with the theoretical predictions, for several azimuthally symmetric magnetized plasma modes as a function of ω_r for $\omega_z/2\pi = 1.13$ MHz and $\Omega/2\pi = 7.608$ MHz. Many different mode frequencies at various values of ω_z have been measured with the Doppler imaging technique, and on very clean clouds agreement between the observed and predicted mode frequencies is typically better than 1%. However, as the percentage of impurity ions increases, the shift between the measured frequency and the value predicted by the single-species theory also increases. Both positive and negative frequency shifts have been observed. We think that these frequency shifts are caused by changes in the cloud shape which perturb the spheroidal geometry of the single-species cloud, arising because impurity ions centrifugally separate from the Be$^+$ [26].
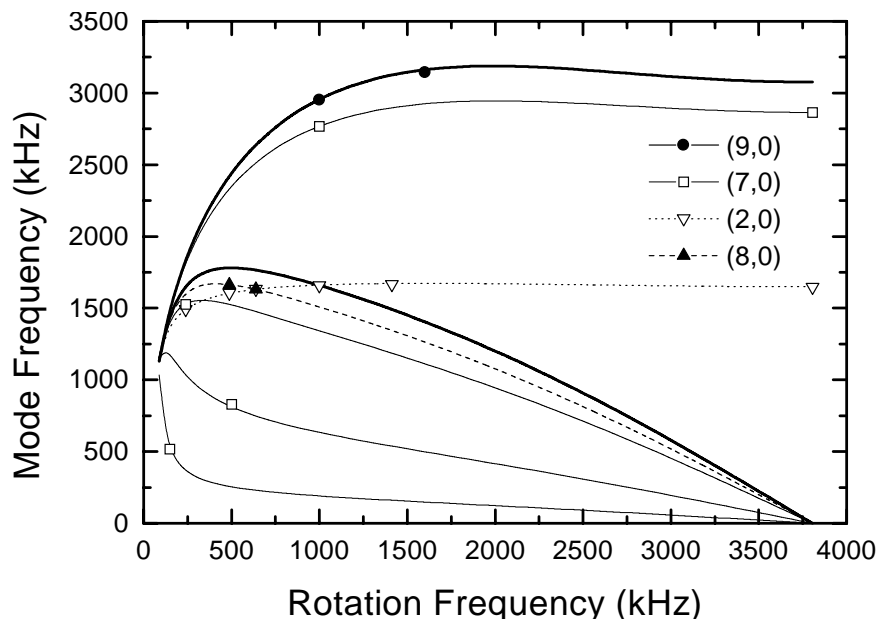
FIGURE 2. Plots of the frequencies of several $m = 0$ magnetized plasma modes as a function of rotation frequency for $\Omega/2\pi$=7.608 MHz and $\omega_z/2\pi$=1.13 MHz. The solid lines are the theoretical predictions and the symbols are experimental measurements. Only the highest frequency $(9,0)$ plasma mode and the second highest frequency $(8,0)$ plasma mode are plotted.
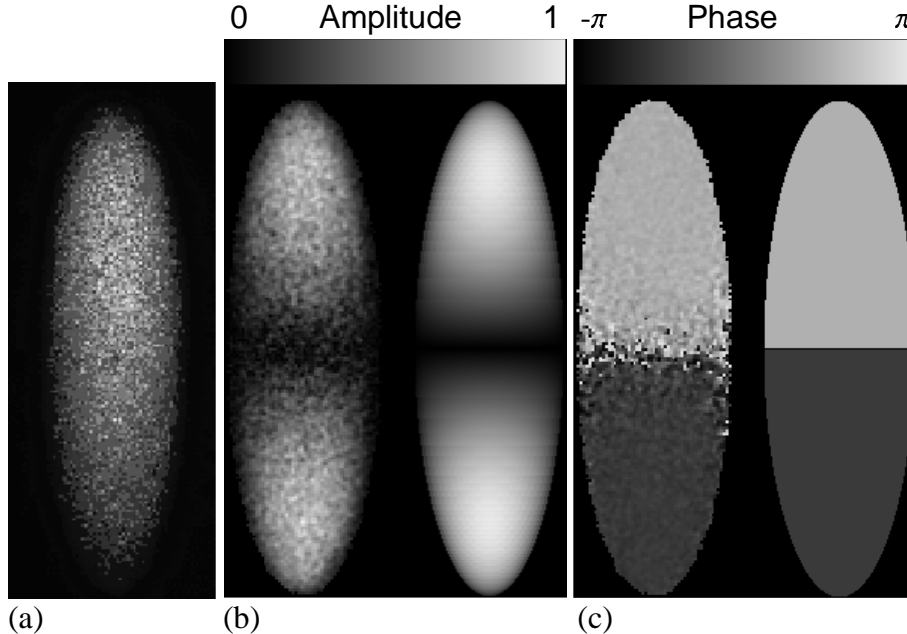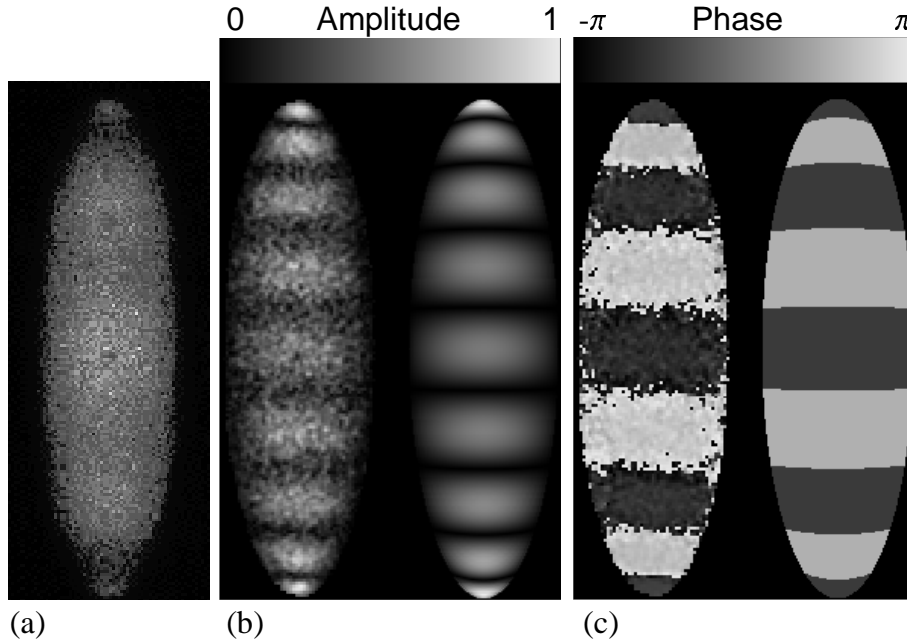
FIGURE 3. (a) Phase-coherent sideview image data obtained on a plasma with $\omega_r/2\pi = 1$ MHz while driving a $(2,0)$ mode at $\omega_{2,0}/2\pi = 1.656$ MHz. The magnetic field and axial laser beam point up. The ion cloud dimensions are $2z_0 = 0.76$ mm and $2r_0 = 0.24$ mm, and the density $n_0 = 2.70 \times 10^9$ cm^{-3}. Comparison of the amplitude (b) and phase (c) extracted from the $(2,0)$ mode in (a) with the predictions of linear theory. The theory predictions for (b) and (c) are on the right. From Ref. [23].

Figure 3 illustrates phase-coherent detection and Doppler imaging of the $(2,0)$ mode. This is one of the simplest modes that is not merely a center-of-mass oscillation of the plasma. In this mode the plasma stays spheroidal but the aspect ratio (and density) oscillate at $\omega_{2,0}$. For $\omega_r \ll \Omega/2$, the oscillation in r_0 is very small, so the mode principally consists of oscillations in z_0 at $\omega_{2,0}$. Ions above the $z = 0$ mid plane oscillate 180° out of phase with ions below $z = 0$.

Figure 3(a) shows one of a sequence of 18 side-view images taken as a function of the phase of the mode drive at $\omega_{2,0}/2\pi = 1.656$ MHz. A movie of the entire sequence is included in Ref. [23]. The plasma's rotation frequency was set to $\omega_r/2\pi = 1$ MHz and the $m = 0$ even drive rms amplitude was 7.07 mV. In the images, the magnetic field and the axial laser beam point up. As expected for the $(2,0)$ mode, the detected fluorescence in the upper half of the plasma is bright when the lower half is dark and vice versa. We analyze the data of Fig. 3(a) by performing a least-squares fit of the intensity at each point to $A_0 + A_{2,0}\cos(\omega_{2,0}t + \varphi_{2,0})$. Figures 3(b) and 3(c) show the resultant images of the measured mode amplitude $A_{2,0}(x,z)$ and phase $\varphi_{2,0}(x,z)$. These are compared with the theoretically predicted values of these quantities. Because the plasma is optically thin, the theoretical predictions were obtained by integrating $\partial \Psi^{lm}/\partial z$ over y. The amplitude of the theoretical prediction is scaled to match the experiment, and both amplitudes are normalized to 1.

From the fitted values of $A_{2,0}$ and A_0 we can estimate the coherent-ion mode velocities if the dependence of the ion fluorescence on velocity (through Doppler shifts) is known. For the low temperatures of this experiment a good approximation is to assume a Lorentzian profile with a full width at half maximum of 19 MHz due to the natural linewidth of the optical cooling transition. With the 20 MHz detuning used in this measurement, we estimate for the data of Fig. 3 that the maximum coherent mode velocity, which occurs at $z = \pm z_0$, is $\sim$1.5 m/s. The spatial and density changes in the plasma spheroid for this excitation are too small to be resolved ($\Delta z/z_0, \Delta n/n_0 < 10^{-3}$). Therefore the observed variation in the fluorescence intensity is entirely due to Doppler shifts induced by the coherent ion velocities of the mode.

We have measured the mode eigenfunctions of a number of different azimuthally symmetric modes including the l=2,3,4,5,7, and 9 modes. Like the data of Fig. 3, good agreement with the predicted eigenfunction amplitude and phase distribution is obtained in the limit of low laser power and drive amplitude. Surprisingly high-order odd modes could be excited with the odd drive on the trap endcaps. Figure 4(a) shows one
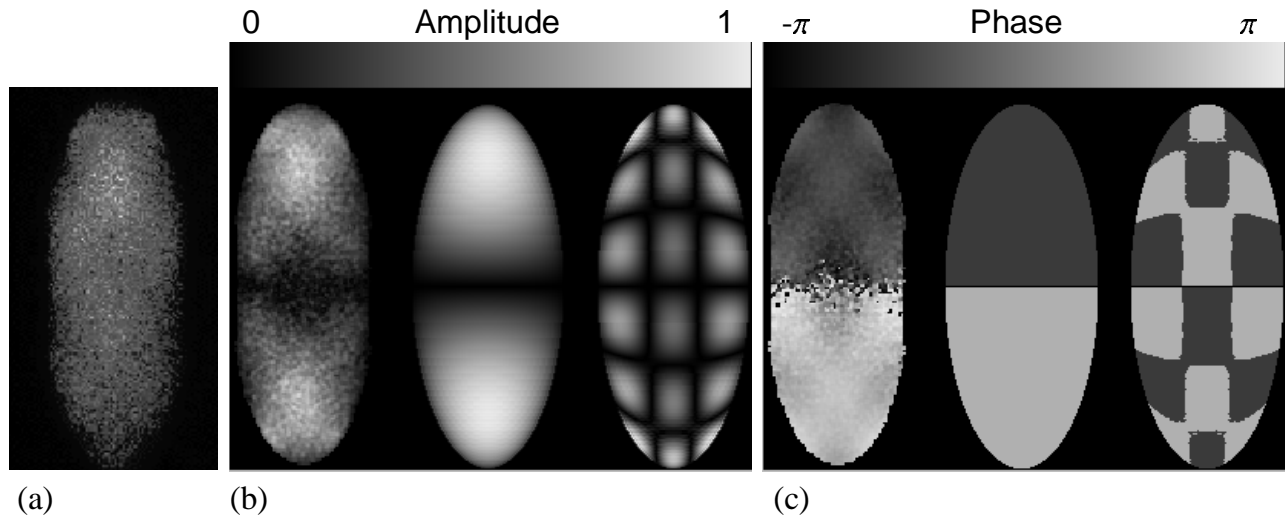
FIGURE 4. (a) Phase-coherent sideview image data obtained on the plasma of Fig. 3 with $\omega_r/2\pi = 1.00$ MHz while driving a $(9,0)$ mode at $\omega_{9,0}/2\pi = 2.952$ MHz. Comparison of the amplitude (b) and phase (c) extracted from the $(9,0)$ mode in (a) with the predictions of linear theory. The theory predictions are on the right. From Ref. [23].

of a sequence of 18 sideview images obtained with the highest frequency $(9,0)$ mode excited by a drive at $\omega_{9,0}/2\pi = 2.952$ MHz. For a given $(l,0)$, the highest frequency magnetized plasma mode does not have any radial nodes. Figures 4(b) and 4(c) show the fitted amplitude and phase from the sequence, along with the predictions from theory. Similar high-order even $(l,0)$ modes are more difficult to excite. The mode eigenfunctions of some of the azimuthally asymmetric ($m=1$ and $m=2$) modes, such as the $(1,1)$, $(2,1)$, $(3,1)$ $(4,1)$, $(6,1)$, $(8,1)$ and $(3,2)$ modes, have also been imaged. In general, the qualitative agreement with the predictions of theory is good.

Figure 5 shows images from a plasma with $\omega_r/2\pi = 638$ kHz driven by an even drive at 1.619 MHz. This case demonstrates the utility of the Doppler imaging diagnostic. These data were initially taken during a survey of the $(2,0)$ mode eigenfunction as a function of the plasma's rotation frequency. Analysis of the phase-coherent data revealed additional, higher-order structure. An examination of the predictions for the mode frequencies revealed that at this particular rotation frequency, as shown in Fig. 2, both the $(2,0)$ mode and an $(8,0)$ mode with a radial node have similar frequencies. Characteristics of both modes are seen in the data. However, subsequent measurements of the $(2,0)$ mode frequency near this crossing indicated that any frequency shifts due to a nonlinear coupling with the $(8,0)$ mode are less than a few kilohertz. The $(2,0)$ mode driven in Fig. 3 occurs near a crossing with a $(9,0)$ mode (see Fig. 2). In this case no evidence for an excitation of a $(9,0)$ is observed, presumably because it is an odd mode which does not couple to even drives, and because there is little or no mode coupling between the $(2,0)$ and $(9,0)$.

Doppler imaging also provides a technique for measuring the damping of plasma modes. This is done by sweeping the frequency ω_{pert} of the sinusoidally time-varying perturbation through a mode frequency, while measuring the mode's resultant amplitude and phase. If the perturbation amplitude is kept low to avoid large amplitude effects the system can be modeled as a damped harmonic oscillator driven by a periodic external force, which has a characteristic lineshape for its amplitude response and a phase difference of π above and below resonance [27].

Figure 6 shows a measurement of the $(2,0)$ mode amplitude and phase response. The axial laser intensity was reduced in an attempt to make mode damping from viscous dissipation dominant over that from laser cooling, and the $z > 0$ upper half of the plasma was blocked off to permit phase-coherent detection without spatial discrimination. At each perturbation drive frequency ω_{pert} the fluorescence intensity was fitted to

FIGURE 5. (a) Phase-coherent sideview image data obtained on a plasma with $\omega_r/2\pi = 638$ kHz while driving with an even drive at 1.619 MHz. At this rotation frequency there is a crossing of the $(2,0)$ mode and an $(8,0)$ mode with a radial node. Comparison of the amplitude (b) and phase (c) extracted from the data in (a) with the predictions of linear theory. The predictions of both the $(2,0)$ and $(8,0)$ modes are given. For this plasma $2z_0 = 0.70$ mm and $2r_0 = 0.29$ mm. From Ref. [23].
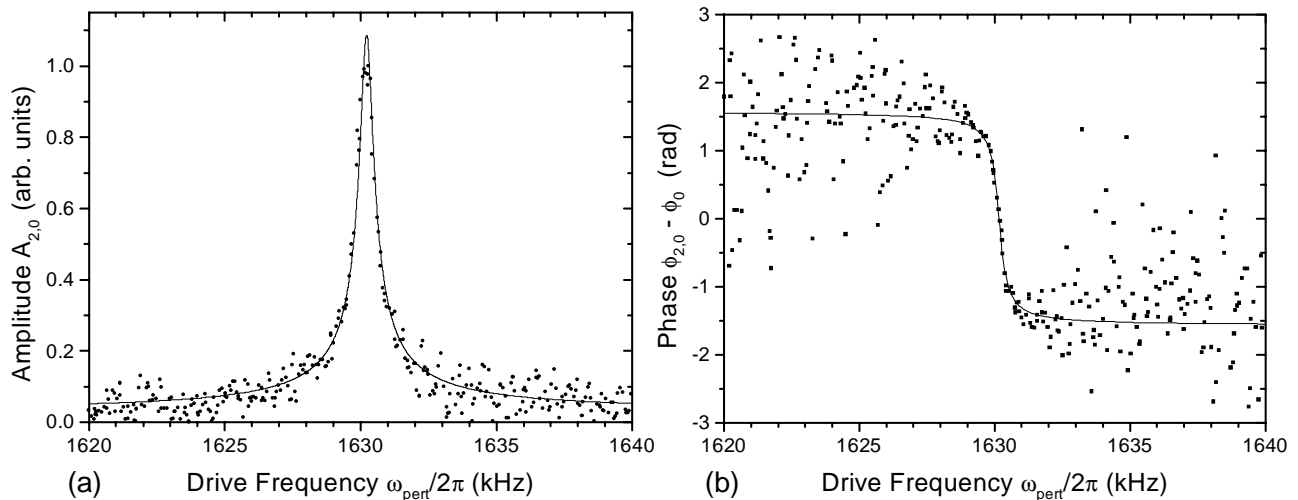
FIGURE 6. Measurement of the $(2,0)$ mode amplitude (a) and phase (b) as a function of perturbation drive frequency. The lines are fits to theory curves for the velocity of a driven, damped harmonic oscillator [27].

7

$A_0 + A_{2,0} \cos(\omega_{pert}t + \varphi_{2,0})$. Figure 6(a) shows the measured amplitude $A_{2,0}$ along with a 4-parameter fit to the damped harmonic oscillator lineshape $a_0 + a_1\omega_{pert}/(\omega_{2,0}\sqrt{(\omega_{pert} - \omega_{2,0})^2 + \lambda^2})$, where λ is the damping coefficient. Figure 6(b) shows the measured phase $\varphi_{2,0}$ along with a 3-parameter fit to $\varphi_0 - \arctan((\omega_{pert} - \omega_{2,0})/\lambda)$. The two fits give damping coefficient values of $\lambda = 1405$ and 1409 s^{-1}. These are consistent with the rates of viscous damping seen in simulations [9].

Angular Momentum Transport From Resonant Modes

In principle, the confinement time of non-neutral plasmas in Penning traps is infinite because angular momentum conservation in an ideal, cylindrically symmetric trap places a constraint on the radial transport of the plasma [28]. In practice radial transport of the plasma always occurs, and at rates which, with ultrahigh vacuum, are greater than can be explained by collisions of the plasma with the neutral background gas. Because the rates of this "ambient" transport increase with increasing static field errors in the trap, it is thought to be caused by couplings between the confining field asymmetries and the plasma [29].

Although ambient transport is at present poorly understood, progress has been made on the related but simpler mechanism of mode-resonant transport. Here, torques are imparted because azimuthally asymmetric plasma modes can have zero frequency in the laboratory frame and hence be excited by the static field errors [6,11,30–32]. Because these modes need to have negative (backward) frequencies in the rotating frame of the plasma to come into resonance with a static field error, any torque they exert will slow the plasma down and hence increase transport. An analysis based on the second law of thermodynamics yields the same result [28].

When the trap walls are well away from the plasma and the ambient field errors are small, as in our experiment, it is particularly easy to study mode-resonant transport. Reference [11] demonstrated that torque and heating of the plasma occur when one of the (2,1) plasma modes is resonant with a static field error produced by a tilt between the trap symmetry axis and the magnetic field. The presence of additional heating resonances at lower rotation frequencies was also noted. We have used Doppler imaging to identify these resonances and find that they arise from $(l,1)$ modes which come into resonance with the tilted-field error. We have also established that they exert a torque when they are resonant. Experimentally this tilt can be applied either mechanically by tilting the trap electrodes, or electrically with $m = 1$ perturbations applied to the compensation electrodes; we find no difference in the transport caused by the two methods.

Figure 7 is a plot of rotation frequency (as determined by side-view images [3]) versus time for a plasma when the trap has been electrically tilted from its aligned value by an amount equivalent to $\sim 5 \times 10^{-4}$ radians of mechanical tilt. Radial transport, which is measured here by decreases in rotation frequency (corresponding in this experimental regime to increases in the plasma radius), is enhanced by roughly a factor of 10 as compared with the aligned case. The rotation frequencies where transport is especially rapid can be identified with the mode resonances indicated on the plot. The lines show the predictions from theory for where the indicated mode has $\omega_{lm} = -\omega_r$, and Doppler imaging was used to verify the identity of these resonant zero-frequency modes. We find that the tilted-field error couples to modes with $m = 1$ and odd axial symmetry. Since with a single-species cloud only the $(2,1)$ is predicted in linear theory to couple with a tilted-field error, the transport displayed in Fig. 7 might require the presence of impurity ions. In ion traps these are usually present at some level, and comprised $\sim 20\%$ of the cloud of Fig. 7.

Because small-amplitude static field errors can be so effective in causing outward transport, it is not surprising that the process can be usefully inverted by actively driving modes which travel faster than the cloud's rotation. With the laser-cooled Be$^+$ plasmas, we have demonstrated mode-resonant inward transport with the (1,1), (2,1), (3,1) and (2,2) modes. The (1,1) is particularly easy to excite, as only an axially uniform rotating dipole field is required, and is useful for driving clouds into the regime where ω_r approaches Ω_c. The mode-resonant technique can do this in a few seconds, while doing the same thing with laser torque takes many seconds, and with the rotating wall perturbation at least several minutes. We note that the (1,1) mode requires an effect to break the separation between the center-of-mass and the internal degrees of freedom of the plasma. In our work, a small number of impurity ions could do this.

In comparison with the rotating wall technique for controlling an ion cloud's rotation frequency [14,15], the mode-resonant technique is less precise. The mechanism by which the rotating wall is believed to work with strongly correlated plasmas is that the plasma comes into equilibrium with rotating distortions of its surface which are imposed by the perturbation. Hence, the torque from a perturbation applied at frequency f_{RW} goes to 0 when $f_{RW} = f_r$, and changes sign about this point. In contrast, the torque imparted by a driven (l,m) mode usually has only one sign and is experimentally observed to depend sensitively upon such parameters
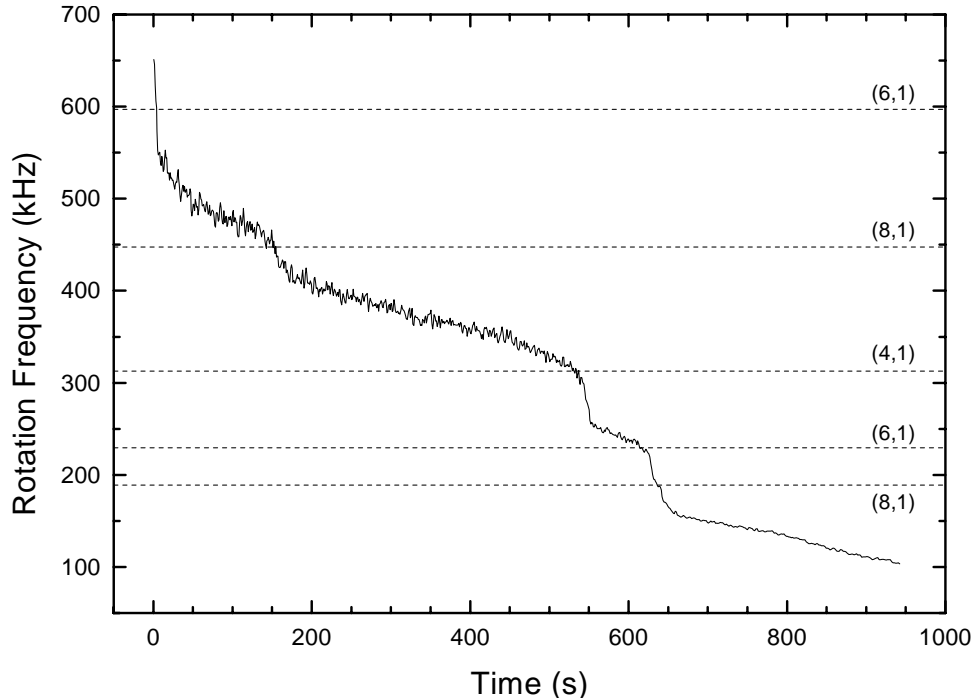
FIGURE 7. Measured plasma rotation frequency vs. time obtained when the trap was electrically tilted ∼5 ×10^{-4} radians from its aligned value. The lines are predictions from theory for where the indicated modes have zero frequency in the lab frame.

as the temperature of the plasma. As a consequence the rotation frequency at which the cloud comes into equilibrium with the mode, which is determined by a balance between the inward mode torque and the outward ambient torque, is difficult to calculate in advance and is experimentally observed to change with variations in the cooling laser power or frequency.

However, an important advantage of mode-resonant coupling is that it can be used to transfer angular momentum to hot (uncorrelated: $\Gamma \ll 1$) plasmas. The phase-locked rotating wall control [14,15] described above has only been demonstrated with laser-cooled plasmas. In contrast, mode-resonant coupling has been used to increase angular momentum in non-neutral plasmas with temperatures up to 5 eV (which is where ionization of neutrals begins to change the density profile). Reference [12] demonstrated inward radial transport of a hot (T=0.9 eV) spheroidal electron cloud through the use of $(l, 1)$ modes. This transport was accompanied by a heating of the electrons, since there were no cooling processes in the experiment. At higher magnetic fields the heating can be balanced by cyclotron radiation cooling; steady-state confinement of uncorrelated electron plasmas in a 4 T field through the application of azimuthally asymmetric modes has recently been demonstrated [33].

SUMMARY AND FUTURE DIRECTIONS

We have described a technique, Doppler imaging, for studying the mode properties of laser-cooled ion plasmas. In general, for the magnetized plasma modes of spheroidal plasmas discussed here, good agreement is obtained between linear theory and the experimental measurements we have made to date. In the future the technique should be a useful tool for studying deviations from the linear theory such as large amplitude frequency shifts, non-linear corrections to the mode eigenfunction, and mode coupling. Because the width of the resonant lineshape of the mode amplitude as a function of the drive frequency provides a measurement of the mode damping, lineshape measurements may be able to provide information on the collisional viscosity of the strongly correlated plasma, about which little is currently known. Enhanced radial transport is observed when modes are resonant with static external perturbations, and future work may permit a quantitative

9

comparison to be made between experiment and theory for this basic transport process. Finally, we described how the plasma angular momentum can be usefully changed through the deliberate excitation of azimuthally asymmetric modes.

ACKNOWLEDGMENTS

REFERENCES

1. Fajans, J., and Dubin, D. H. E., *Non-Neutral Plasma Physics II*, New York: AIP, 1995.
2. Malmberg, J. H., and O'Neil, T. M., *Phys. Rev. Lett.* **39**, 1333–1336 (1977).
3. Brewer, L. R., *et al.*, *Phys. Rev. A* **38**, 859–873 (1988).
4. Bollinger, J. J., Wineland, D. J., , and Dubin, D. H. E., *Phys. Plasmas* **1**, 1403–1414 (1994).
5. Dubin, D. H. E., **66**, 2076–2079 (1991).
6. Bollinger, J. J., *et al.*, *Phys. Rev. A* **48**, 525–545 (1993).
7. Greaves, R. G., and Surko, C. M., *Phys. Plasmas* **4**, 1528–1543 (1997).
8. Holzscheiter, M. H., *et al.*, *Phys. Lett. A* **214**, 279–284 (1996).
9. Dubin, D. H. E., and Schiffer, J. P., *Phys. Rev. E* **53**, 5249–5267 (1996).
10. Dubin, D. H. E., *Phys. Rev. E* **53**, 5268–5290 (1996).
11. Heinzen, D. J., *et al.*, *Phys. Rev. Lett.* **66**, 2080–2083 (1991).
12. Mitchell, T. B., Ph.D. thesis, University of California at San Diego, 1993, pp. 58–61.
13. Huang, X.-P., *et al.*, *Phys. Rev. Lett.* **78**, 875–878 (1997).
14. Huang, X.-P., Bollinger, J. J., Mitchell, T. B., and Itano, W. M., *Phys. Rev. Lett.* **80**, 73–76 (1998).
15. Huang, X.-P., Bollinger, J. J., Mitchell, T. B., and Itano, W. M., *Phys. Plasmas* **5**, 1656–1663 (1998).
16. Weimer, C. S., Bollinger, J. J., Moore, F. L., and Wineland, D. J., *Phys. Rev. A* **49**, 3842–3853 (1994).
17. Tinkle, M. D., Greaves, R. G., and Surko, C. M., *Phys. Plasmas* **2**, 2880–2894 (1995).
18. Greaves, R. G., Tinkle, M. D., and Surko, C. M., *Phys. Rev. Lett.* **74**, 90–93 (1995).
19. Driscoll, C. F., *Phys. Rev. Lett.* **64**, 1528–1543 (1990).
20. Tan, J. N., Bollinger, J. J., Jelenković, B., and Wineland, D. J., *Phys. Rev. Lett.* **75**, 4198-4201 (1995).
21. Itano, W. M., *et al.*, *Science* **279**, 686–689 (1998).
22. Here ω_{lm} is the mode frequency in a frame rotating with the plasma. For the $m = 0$ modes discussed here this distinction is not necessary because their frequency is the same in either the laboratory or rotating frame.
23. Mitchell, T. B., Bollinger, J. J., Huang, X.-P., and Itano, W. M., *Opt. Exp.* **2**, 314–322 (1998).
24. Information on the mode eigenfunction can be obtained from the side-view images even when there is a change in the phase-averaged ion fluorescence. However, the images may no longer provide a linear measure of the mode axial velocity.
25. Thompson, R. C., *et al.*, *Phys. Scripta* 24–33 (1997).
26. Larson, D. J., *et al.*, *Phys. Rev. Lett.* **57**, 70–73 (1986).
27. Landau, L. D., and Lifshitz, E. M., *Mechanics and Electrodynamics*, Oxford: Pergamon Press, 1972, pp. 68–70.
28. O'Neil, T. M., and Dubin, D. H. E., *Phys. Plasmas* **5**, 2163–2193 (1998).
29. Driscoll, C. F., Fine, K. S., and Malmberg, J. H., *Phys. Fluids* **29**, 2015–2017 (1986).
30. Driscoll, C. F., and Malmberg, J. H., *Phys. Rev. Lett.* **50**, 167–170 (1983).
31. Keinigs, R., *Phys. Fluids* **27**, 1427–1433 (1984).
32. Eggleston, D. L., O'Neill, T. M., and Malmberg, J. H., *Phys. Rev. Lett.* **53**, 982–984 (1984).
33. Anderegg, F., Hollmann, E. M., and Driscoll, C. F., "Rotating Field Confinement of Pure Electron Plasmas Using Trivelpiece-Gould Modes," submitted to *Phys. Rev. Lett.*